CHEMISTRY
A EUROPEAN JOURNAL

DOI: 10.1002/chem.200600825

In Vitro Study of Magnesium-Calcite Biomineralization in the Skeletal Materials of the Seastar *Pisaster giganteus*

Subramanyam Gayathri,[a] Rajamani Lakshminarayanan,[a] James C. Weaver,[b] Daniel E. Morse,[b] R. Manjunatha Kini,[c] and Suresh Valiyaveettil*[a]

Abstract: The mechanisms of formation of biogenic magnesium-rich calcite remain an enigma. Here we present ultrastructural and compositional details of ossicles from the seastar *Pisaster giganteus* (Echinodermata, Asteroidea). Powder X-ray diffraction, infrared spectroscopy and elemental analyses confirm that the ossicles are composed of magnesium-rich calcite, whilst also containing about 0.01% (w/w) of soluble organic matrix (SOM) as an intracrystalline component. Amino acid analysis and N-terminal sequencing revealed that this mixture of intracrystalline macromolecules consists predominantly of glycine-rich polypeptides. In vitro calcium carbonate precipitation experiments indicate that the SOM accelerates the conversion of amorphous calcium carbonate (ACC) into its final crystalline product. From this observation and from the discovery of ACC in other closely related taxa, it is suggested that substitution of magnesium into the calcite lattice through a transient precursor phase may be a universal phenomenon prevalent across the phylum echinodermata.

Keywords: biomineralization · crystal growth · echinoderms · magnesium calcite · mesophases

Introduction

Biological systems have developed complex and intriguing strategies to deposit inorganic minerals in their structural frameworks.[1–4] Several groups of marine invertebrates utilize $CaCO_3$ as a skeletal material, despite its intrinsically brittle nature, and the resulting structures, which typically incorporate small percentages of macromolecular components, exhibit complex morphologies and can be remarkably tough, often outperforming manmade ceramics. Such biogenic forms of $CaCO_3$ are created with the formation of intricate structures difficult to reproduce through conventional ceramic syntheses. Members of the phylum Echinodermata (seastars, brittle stars, sea urchins, sea cucumbers and sea lilies) possess mesodermally derived, subepidermal endoskeletons consisting of numerous individual platelike structures called the ossicles,[5–8] each of which consists of a single crystal of three-dimensionally bicontinuous porous magnesium calcite. Aizenberg et al. have shown that the ossicles of some species of brittle stars (such as *Ophiocoma wendtii*) are modified to function as arrays of microlenses aiding in photodetection, highlighting the potential multifunctional characteristics of these materials.[7–8] Many of these skeletal elements contain significant amounts of magnesium, varying from ≈2 mol% to 40 mol%.[9] Such high levels of isomorphous replacement with Mg^{2+} ions in the calcite lattice are difficult to achieve under ambient conditions (up to 10 mol% Mg can be substituted into the calcite lattice under synthetic conditions).

Falini et al. reported Mg contents of about 14 mol% in calcium carbonate crystallized from water/alcohol mixtures,[10] and X-ray crystal structure refinements of two synthetic calcite single crystals containing 3.1 and 5.7 mol% Mg have also been reported.[11] It has been suggested that large

[a] S. Gayathri, R. Lakshminarayanan, Prof. S. Valiyaveettil
Department of Chemistry, National University of Singapore
3 Science Drive 3, Singapore 117543 (Singapore)
Fax: (+65) 6779-1691
E-mail: chmsv@nus.edu.sg

[b] J. C. Weaver, Prof. D. E. Morse
Institute for Collaborative Biotechnologies and
Materials Research Laboratory
University of California at Santa Barbara
Santa Barbara, CA 93106 (USA)

[c] Prof. R. M. Kini
Department of Biological Sciences
National University of Singapore
Science Drive 4, Singapore 117543 (Singapore)

Supporting information for this article is available on the WWW under http://www.chemeurj.org/ or from the author: FTIR spectra of the $CaCO_3$ precipitated in the presence of BSA in the crystallization medium showing the formation of predominantly aragonitic phase of the mineral with time.

thermal vibrations may be the main factor influencing the relative thermodynamic stability of magnesium calcite. Loste et al. crystallized magnesium calcites containing up to 47 mol% Mg from aqueous solutions containing Mg (without organic additives) under conditions of high supersaturation.[12] These experiments demonstrated that a progressively more stable ACC was produced with increasing Mg/Ca ratios in solution, subsequently transforming into the crystalline phase to yield a magnesium-rich calcite lattice. Crystallization of stable high-magnesium calcites in the presence of organic additives has also been reported.[13]

Biological systems have evolved strategies for high magnesium incorporation and stabilization, yielding favourable material properties. In sea urchin spines, for example, the inhomogeneous distribution of Mg^{2+} impedes crack propagation, thus enhancing fracture resistance.[14–16] Improved understanding of the role of Mg^{2+} and its incorporation into the calcite lattice has thus attracted considerable interest among materials scientists.

Politi et al.[17] have shown that regeneration of sea urchin spines takes place through an intermediate amorphous calcium carbonate phase. Since all echinoderms produce similar macroporous skeletal materials, the authors suggested that this mechanism may be the same in other members of the phylum.

The objective of our study was to understand the mechanisms controlling ossicle biosynthesis in seastars and to gain further insight into the mechanism of Mg^{2+} incorporation in the calcite lattice. Here we report the ultrastructure and composition of ossicles from the temperate Eastern Pacific seastar, *Pisaster giganteus*, as analysed by X-ray powder diffraction, scanning electron microscopy and energy dispersive spectroscopy. This species is particularly useful for such studies, thanks to its abundance, unusually large size (frequently >60 cm overall diameter) and high ossicle content. Components of the soluble organic matrix (SOM) present as the intracrystalline component were purified and characterized, and their effects on the precipitation of calcium carbonate were investigated in detail.

Results and Discussion

Characterization of the ossicles: The ossicles for investigation were obtained by bleach treatment of the seastar to remove all associated living tissue and other organic impurities. Figure 1 shows a scanning electron micrograph of the ossicle surface. These images reveal that the ossicles possess an open framework structure containing macropores of 6–15 μm in size, with curved surfaces.

Figure 2A shows the XRD powder pattern of the ossicles. The positions of the diffracted peaks for the ossicles are shifted to longer 2θ values than seen in the pure calcite powder standard, suggesting a significant contraction in the unit cell volume.[18a,b] FTIR spectra indicate that the ν_4 in-plane bending and ν_2 out-of-plane bending vibrations of the carbonate group are shifted to 719 and 877 cm^{-1}, respectively, for the ossicles, in relation to 713 and 875 cm^{-1} for the synthetic calcite crystals (Figure 2B). The ν_4 peak was broadened [full width at half maximum (FWHM) $\approx$21 cm^{-1}, relative to 12 cm^{-1} for the pure calcite] and showed an additional weak band around 1088 cm^{-1}. These observations suggest that the ossicles contain significant amounts of foreign cations in the calcite lattice. EDS analysis indicated the presence of Mg ions, suggesting that the ossicles are magnesium-rich calcites (Figure 2C). It had previously been observed that the wavenumber of the ν_4 absorption band observed in the FTIR varies linearly with the amount of magnesium in the magnesium calcite solid solutions.[18c] From the equation derived from those observations [$\nu_4\,(cm^{-1}) = 39.40\,X_{Mg}+712.20$] the predicted content of Mg in the ossicles was found to be about 19.5 mol%, which is in close agreement with the amount of magnesium estimated by atomic absorption spectroscopy [ca. 20.3(2) mol%]. The presence of such high levels of magnesium ions in the calcite lattice accounts for the significant shift in the XRD powder pattern and the ν_4 absorption peak in the FTIR spectra. The Mg content estimated from the shift of the XRD peaks was found to be 14.6 mol%.

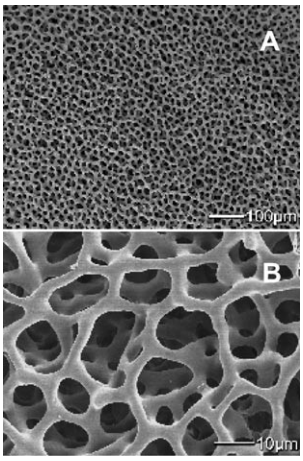

Figure 1. Scanning electron micrograph of *Pisaster giganteus* ossicle surface: scale bar in A represents 100 μm and in B 10 μm.

Bulk composition, purification and characterization of the intracrystalline SOM: To isolate the intracrystalline SOM, the mineral was dissolved in acetic acid (30%) at 4°C, dialysed extensively against MilliQ water for 48 h and lyophilized. The yield of the SOM was found to be about 0.01% of the biomineral by weight, while the UV spectrum of the lyophilized extract displayed a strong absorption maximum at 216 nm and a small hump around 280 nm, indicating that the SOM contains proteins with small amounts of aromatic amino acid residues (Figure 3A). Excitation at 280 nm gave an emission maximum at 354 nm, indicating the exposed nature of the fluorophores (Figure 3A).

FTIR spectra of the SOM revealed the diagnostic amide I band at 1620 cm^{-1}, characteristic of a β-sheet structure, together with the amide II band at 1548 cm^{-1}, suggesting that

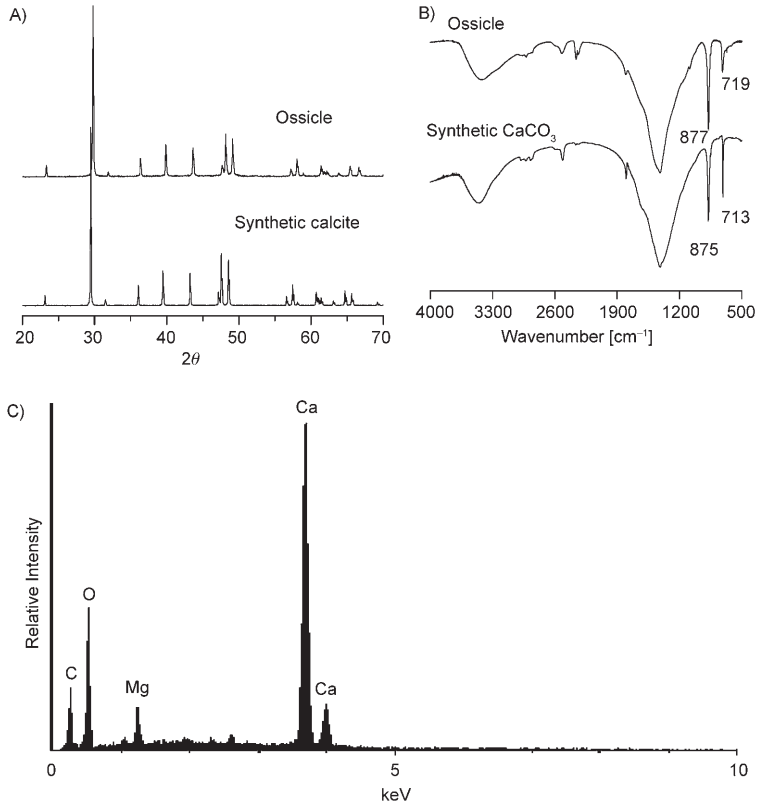

Figure 2. A) XRD spectrum of ossicle powder showing a higher-angle shift in 2θ (relative to a calcium carbonate standard) due to magnesium doping in the calcite lattice. B) Infrared spectrum of ossicle powder showing a shift of the calcitic resonance bands due to the presence of Mg. C) EDS spectra of the ossicle powder showing the presence of high Mg in addition to Ca, C and O.

the SOM was predominantly composed of proteins (Figure 3B). The lack of a strong absorption band in the 1000 to 1150 cm^{-1} region suggests the absence of sugar moieties in the SOM.[19] In contrast, the spectrum of chicken ovomucoid (a highly glycosylated α-helix protein) shows the amide I band around 1668 cm^{-1}. Comparison of these spectra and that of chicken lysozyme (a non-glycosylated protein) indicated that proteins present in the intracrystalline SOM probably adopt a coiled or β-sheet conformation. Amino acid compositional analysis indicated that ≈65% of the mass of the SOM is represented by nonpolar amino acids, including glycine (30.8%), alanine (10.1%) and proline (10.3%) in significant amounts (Table 1).

To characterize it further, a portion of the SOM was fractionated by reversed-phase high-performance liquid chromatography (RP-HPLC) (Figure 3C). The elution profile exhibited a diffuse band at 45% buffer B (0.1% trifluoroacetic acid in 80% acetonitrile), together with clusters of minor fractions in the range 25–40% buffer B. These fractions were labelled according to the decrease in retention time and their molecular masses were determined by MALDI-TOF MS. Fraction A1 showed a spectrum with a mass around 5289; the masses of the other smaller fractions are listed in Table 2,

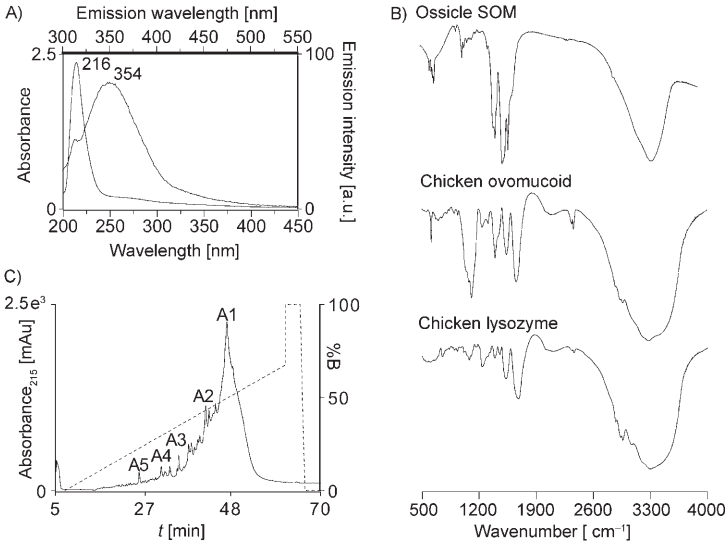

Figure 3. A) UV/Vis absorption (λ_{max} = 216 nm) and emission (λ_{max} = 356 nm) spectra of SOM from *P. giganteus* ossicles. B) Infrared spectrum of the crude extract from the ossicles showing amide I (1620 cm^{-1}) and II (1548 cm^{-1}) resonance bands of proteins, in relation to spectra of chicken ovomucoid and chicken lysozyme. C) RP-HPLC profile of the ossicle SOM showing five major fractions A1–A5.

Table 1. Amino acid composition of the ossicle SOM.

Amino acid	Composition [mol%]
Asx	9.67
Glx	8.09
Ser	6.49
Gly	30.83
His	1.04
Arg	2.31
Thr	3.51
Ala	10.14
Pro	10.28
Tyr	1.89
Val	5.67
Met	1.30
Ile	1.61
Leu	2.64
Phe	3.68
Lys	0.85

Table 2. Partial amino acid sequences of the fractions (A1–A5) from RP-HPLC of the crude extract.

Fraction	Molecular mass	Sequence
A1	5289	IGNPQLPAVPGANADPSKVGGGG
A2	6385.4	VGGPGGPAVPAGXXNDNADDXGGXT
A3	3654.2	VGGPGGV(P)AAG
A5	6014.9	VVGXGAAAGGXNDNADDGGXDTPDDSPGGPYV

together with partial amino terminal sequences of A1 and the other minor fractions. No significant similarity was found between these sequences and any known proteins in the NCBI or FASTA protein databases, suggesting that these peptides are new and specific to the organic matrix of seastar ossicles. Consistent with the amino acid compositional analyses, the amino acid sequences of the purified fractions indicated that they consist of glycine-rich polypeptides.

In vitro $CaCO_3$ mineralization experiments: These experiments were directed towards the determination of the role of the intracrystalline SOM in the formation of high-magnesium calcite. Calcium carbonate was precipitated in the presence both of the macromolecules extracted from the seastar ossicles and of a high concentration of magnesium ions (Ca/Mg 1:1) in solution. The precipitates were collected after different time intervals and characterized by FTIR and electron microscopy. The control experiments (without any added SOM) yielded numerous spherical particles measuring about 3 μm in diameter after 1 h of crystallization (Figure 4).

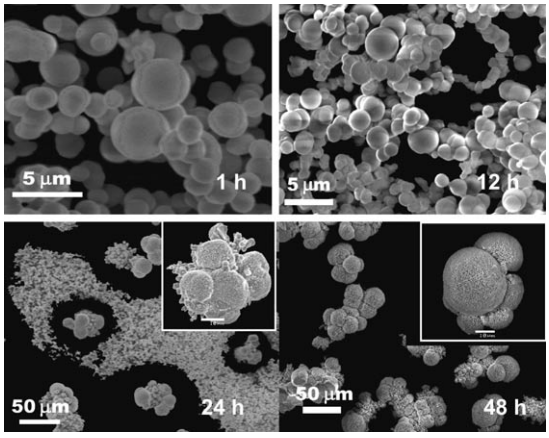

Figure 4. Representative electron micrographs of the calcium carbonate precipitates formed in the presence of magnesium and in the absence of the ossicle SOM at various intervals. Over time, the amorphous $CaCO_3$ spheres transform into fluffy aragonitic structures.

FTIR analyses of these spheres showed a split in the asymmetric stretches of the carbonate ion at 1425 and 1490 cm^{-1} (ν_3), a sharp ν_2 absorption band at 866 cm^{-1} and a broad band around 700 cm^{-1}, characteristic of an ACC phase (Figure 5). When sampled after 2 h and up to 12 h, the precipitates exhibited similar morphological traits. The infrared spectrum at 2 h displayed peaks characteristic of ACC, whereas the 12 h spectrum showed the occurrence of small amounts of calcite co-occurring with ACC, as inferred from the concomitant sharpening of the ν_2 band at 873 cm^{-1} and slight narrowing of the ν_4 band at 713 cm^{-1}.

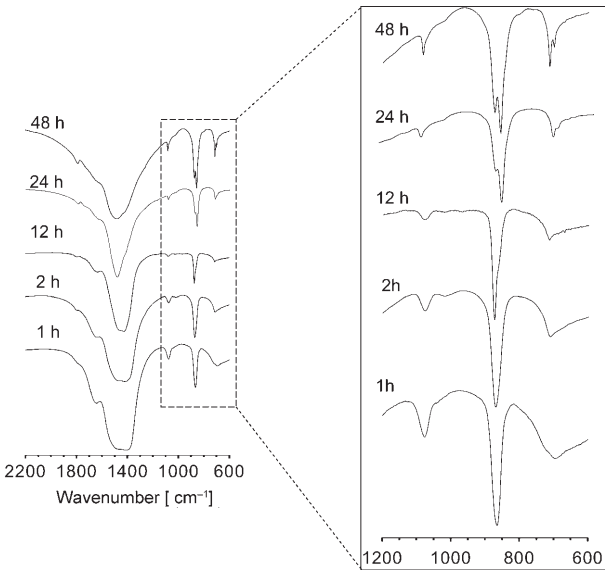

Figure 5. FTIR spectra of the $CaCO_3$ precipitates obtained in the absence of SOM as a function of time. Control experiments suggest that the initially formed ACC was predominantly transformed into aragonite crystals. [Note the intensity of the ν_2 band at 856 cm^{-1} relative to 873 cm^{-1} for the 48 h spectrum.]

The transformation into the crystalline phase was enhanced after about 24 h (Figure 4), by which time the spherical amorphous particles had grown into polycrystalline clusters with a fluffy appearance. The FTIR spectrum of this precipitate (sampled at 24 h) showed formation of the predominantly aragonitic mineral phase from the splitting of the ν_4 band (700 and 713 cm^{-1}) and the appearance of the ν_2 band at 856 cm^{-1}—coexisting with small amounts of calcite (weak band at 873 cm^{-1}). The complete transformation to the crystalline phase occurred within 48 h (Figure 4). From the IR spectral data (Figure 5), this final crystalline phase was found to contain a mixture of calcite and aragonite. Aragonite was found to be the predominant product from the relative intensity of the ν_2 absorption band (856 versus 873 cm^{-1}). This is not surprising, given the presence of high concentrations of magnesium in the crystallization medium,[12,20–26] which stabilizes ACC[20] and increases calcite solubility. Estimation of Mg contents in the precipitates by elemental analyses (ICP-OES; Table 3) revealed a drop in Mg content from 20 mol% after 1 h to 7.69 mol% after 48 h. This is to be expected, as the aragonite formed after

Table 3. Estimation of magnesium contents (ICP-OES) in the $CaCO_3$ precipitates obtained in the absence and presence of the ossicle SOM.

Crystallization time [h]	Control [%]	With SOM [%]
1	20.08	23.33
2	15.63	20.31
12	8.35	10.25
48	7.69	7.20

longer intervals contains no Mg in its lattice and hence reflects the lower Mg content of the precipitates.

In marked contrast, addition of SOM (100 $\mu g\,mL^{-1}$) into the crystallization milieu had a profound influence on the precipitation of ACC and its subsequent transformation into the crystalline phase (Figure 6). In the early stages of growth (30 min), the formation of islands of thin films of AAC was observed. Spindle-shaped crystals emerged from these patches of islets after 1 h (Figure 6) and were surrounded by a network of nanometer-sized particles. After a longer period (2 h) the size of the spindle-shaped crystals had increased, whilst after 12 h, a transformation from the spindle-shaped crystals into dumbbell-shaped crystals with a concomitant and progressive increase in size was observed. FTIR spectra of the mineral formed after 1 h displayed a slight broadening of the 713 cm^{-1} (ν_4) and sharp 871 cm^{-1} (ν_2) absorption peaks indicating that the mineral phase contained predominantly calcite with a small amount of an ACC phase (Figure 7). With time, the ν_4 absorption peak (713 cm^{-1}) became narrow, indicating the transformation from ACC into predominantly magnesium calcite. Elemental analyses of the precipitates at 1 h, 2 h and 12 h showed higher Mg incorporation than had been seen in the $CaCO_3$ precipitates formed in the absence of the SOM (Table 3). FTIR analyses of the precipitates at 24 h and 48 h showed the occurrence of small amounts of aragonite, although the major product obtained was magnesium calcite. [In Figure 7 note the absence of splitting of the 713 cm^{-1} band and the relative intensities of the 873 cm^{-1} versus 856 cm^{-1} bands, in relation to the control experiments in Figure 5.] Elemental analysis of the completely transformed crystals indicated a magnesium content of about 7.2 mol%. The FTIR spectral peak locations and the polymorph formed at different stages of the study are summarized in Table 4.

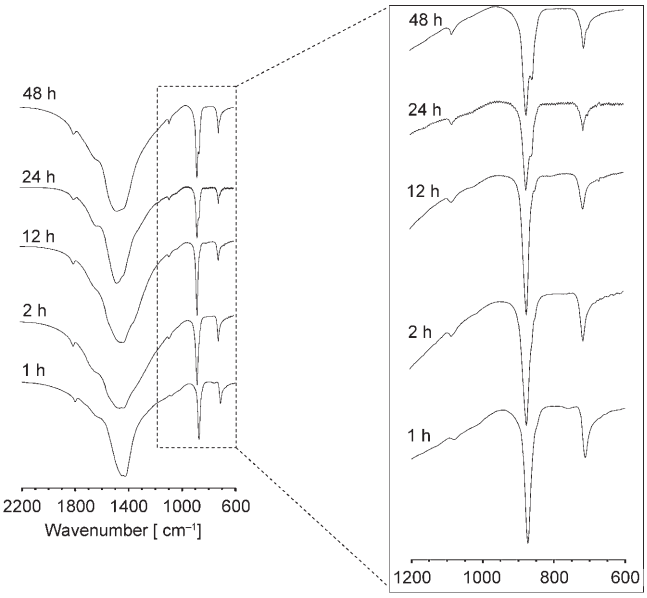

Figure 7. FTIR spectra of the $CaCO_3$ precipitates obtained in the presence of ossicle SOM. [Note the absence of splitting of the ν_4 absorption band at 713 cm^{-1} and the relative intensity of ν_2 absorption at 873 cm^{-1} relative to 856 cm^{-1}].

From these in vitro experiments it is conceivable that the presence of the SOM alters the kinetics of transformation from ACC to the crystalline calcite phase and influences the crystal morphology. Experiments with BSA as a negative

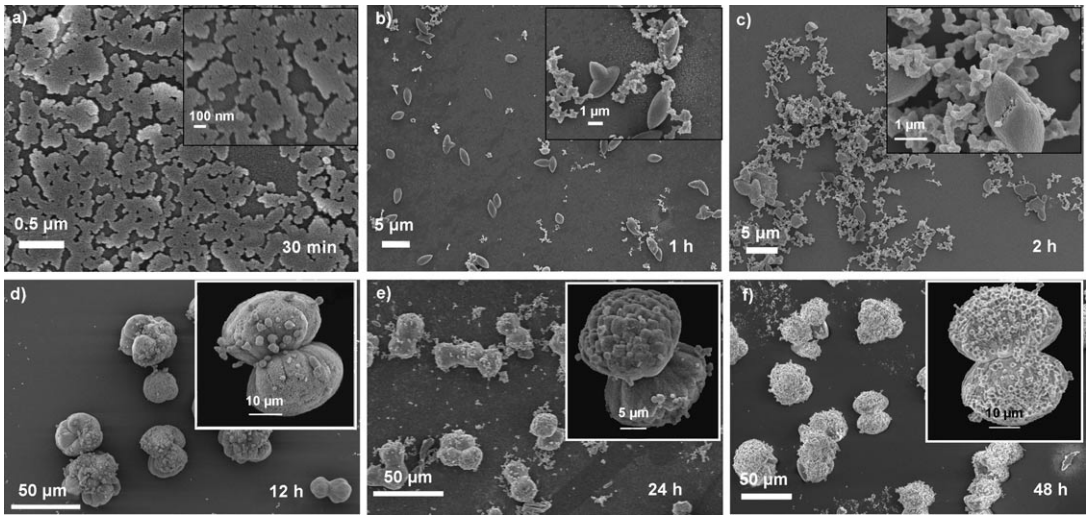

Figure 6. Representative electron micrographs of the calcium carbonate precipitates formed in the presence of ossicle SOM. The initial ACC film transforms through elongated ellipsoids into dumbbell-shaped magnesium calcite crystals.

Table 4. FTIR peak positions in wavenumbers [cm^{-1})] and the polymorph of $CaCO_3$ precipitated in vitro in the absence and presence of ossicle SOM.

t [h]	Control				Ossicle SOM			
	ν_1	ν_2	ν_4	Polymorph	ν_1	ν_2	ν_4	Polymorph
1	1078	866	698 (v br)[a]	*ACC*	1082	873	713 (br)	ACC (less)+*calcite* (major)
2	1078	871	713 (v br)	*ACC*+calcite (traces)	1083	871	713	*calcite*
12	1080	873	715 (br)[b]	*ACC* (major)+calcite (less)	1083	871	715	*calcite*
24	1082	*858*,[d] 873	700, 713	ACC (traces)+calcite (less)+*aragonite* (major)	1082	858 (w)[c], *873*	700 (w), *713*	*calcite* (major)+aragonite (traces)
48	1082	*856*, 873	700, 713	calcite (less)+*aragonite* (major)	1083	858 (w), *873*	700 (w), *713*	*calcite* (major)+aragonite (traces)

[a] v br = very broad, [b] br = broad, [c] w = weak, [d] italics = dominant band of the two.

control in place of the crude ossicle extract were performed: sampling at 1 and 2 h revealed a mixture of amorphous and calcite phases, which was eventually transformed into a mixture of calcite and aragonite crystals after 12 h of crystallization, as confirmed from the FTIR spectra (see Supporting Information, Figure S1). The predominant mineral formed at 12 h was aragonite (as inferred from the relative intensity of the ν_2 band at 856 cm^{-1}), which further confirms the capacity of the SOM to promote the formation of magnesium calcite, relative to aragonite.

It can be inferred that the SOM in the crystallization medium counters the Mg-induced transformation from ACC into aragonite by decreasing the stability of the ACC and increasing the stability of the magnesium-doped calcite. In this process, dissolution of ACC and recrystallization of aragonite may be completely bypassed. Magnesium ions form very strong bonds with water molecules, and the resulting hydration spheres increase the degree of supersaturation in the medium, resulting in the precipitation of amorphous phases.[9] It is possible that the components in the SOM may chelate magnesium ions, disrupting the hydration spheres and reducing the supersaturation in the medium, thereby potentially decreasing the stability of the amorphous phase and accelerating transformation into the crystalline phase.

Transient ACC phases have recently been observed during sea urchin larval spicule formation in *Paracentrotus lividus* and *Strongylocentrotus purpuratus*.[24] Emphasizing the importance of SOM in this process, in vitro studies showed that SOM extracted during the early stages (when the larval spicule consists of a mixture of ACC and calcite phases) induced the precipitation of ACC, while SOM extracted at a later stage (when the spicule is completely crystalline) did not induce ACC formation (despite the great similarity of the amino acid compositions of the SOMs isolated from these two growth stages).[24] Our studies on the seastar *P. giganteus*, which belongs to the same phylum, confirm the prevalence and importance of this mechanism for the control of crystal growth. The SOM facilitated the transformation of a metastable amorphous phase into a stable magnesium calcite phase. The relatively low levels of incorporation of magnesium ions into the calcite crystals obtained from in vitro crystallization experiments highlight the difficulty involved in simulating the microenvironment and control systems identical to those in the biological system. Extraction of the SOMs at various stages of ossicle formation and investigation of their influence on the precipitation of magnesium calcite may provide clues as to the detailed mechanisms governing the biological formation of high-magnesium calcite. Further investigations with this system are underway.

Conclusion

Improvements in understanding the biomineralization processes in the seastar skeleton may provide new insights into the molecular mechanisms involved in the formation of high-magnesium calcites. The ossicles of the seastar *P. giganteus* are unusual (in relation to synthetic and geological calcites) in their composition, containing about 20 mol% Mg incorporated in the calcite lattice and about 0.01 weight% of organic macromolecules. The morphology of the ossicles as inferred from SEM reveals a bicontinuous, thick-walled, porous network. The SOM extracted from the ossicles contains glycine-rich polypeptides with sequences never seen before. The results of our in vitro crystallization experiments indicate that the formation of magnesium-rich calcites can occur through transformation of an amorphous precursor phase. The intramineral seastar proteins were found to influence selectively the polymorphs, compositions and morphologies of the crystals grown in this system.

Experimental Section

Characterization of the ossicles: For morphological characterization of the ossicles (isolated as described immediately below), the samples were mounted on an aluminium stub with double-sided carbon tape, sputter-coated with gold and examined with a JEOL JSM 6300 F scanning electron microscope (SEM) at 5 kV. Energy-dispersive spectroscopic analysis (EDS) of the ossicles (uncoated) was performed with an IXRF Systems EDS instrument attached to a Tescan Vega TS 5130 MM SEM. X-ray diffraction data for the ossicle powder and for a pure $CaCO_3$ mineral standard were collected by use of a D5005 Siemens X-ray diffractometer with $Cu_{K\alpha}$ radiation at 40 kV and 40 mA with a 2θ scanning range between 20 to 70° at a step size of 0.04°. Elemental analyses were carried out with a Thermo Jarrel Ash Duo Axis inductively coupled plasma optical emission spectroscope (ICP-OES). Powdered ossicles (0.5 mg) dissolved in HCl (6 N, 1 mL) and made up to 10 mL with Millipore water was used for the elemental analysis. Triplicate experiments were performed and the average value was taken. The infrared spectroscopic measurements were performed on a Bio-Rad FTS 165 FTIR spectrophotometer with small amounts of the ossicle powder mixed with KBr powder to form a pellet.

Extraction of the soluble organic matrix (SOM) from the seastar ossicles: Ossicles from *P. giganteus* were isolated by sodium hypochlorite treatment of the freshly collected animals, followed by thorough washing with

water. The remaining material (which consisted entirely of the cleaned ossicles) was decalcified with acetic acid (30%) for 2 d at 4°C, filtered and centrifuged. The supernatant was dialysed with Snake Skin pleated dialysis tubing (Pierce) 3500 MWCO membrane at 4°C. The dialysed solution was then freeze-dried and lyophilized to obtain the SOM, which was stored frozen for future use.

Bulk composition analyses: UV/visible spectra of the SOM dissolved in water were recorded from 190 to 600 nm on a Shimadzu 3101 PC spectrophotometer. A background spectrum for water was measured before recording the sample. The fluorescence emission spectrum of the SOM dissolved in water was measured on a Shimadzu RF-5301 PC spectrophotometer with the emission and excitation band passes set at 3 nm. The excitation wavelength was set at 280 nm and the spectra were recorded from 200 to 600 nm. The FTIR spectra of the extracted SOM, chicken ovomucoid (Sigma Aldrich) and chicken lysozyme (Sigma Aldrich) were recorded at 4 cm^{-1} resolution with 32 scans in the wavenumber range of 4000–400 cm^{-1} on a Bio-Rad FTS 165 FTIR spectrophotometer with small amounts of the sample in a KBr pellet.

Amino acid analysis: To determine the amino acid compositions of the crude intracrystalline extracts, the sample (300 μg) was hydrolysed in HCl (6 N) in vacuo at 110°C for 24 h. The hydrolysed products after evaporation of HCl were separated on a Pico-tag column (3.9 mm × 15 cm), derivatized post-column with phenyl isothiocyanate and detected at 254 nm by use of a Waters 2487 Dual Wavelength Absorbance detector at the Advanced Protein Technology Centre, Hospital for Sick Children, Toronto (Canada).

Purification of the intramineral proteins: The crude extract was fractionated on a Jupitor C18 reversed-phase column (10 μ, 250 mm × 4.6 mm) with AKTÄ Explorer 10 (Amersham Biosciences). The column was equilibrated with TFA (0.1%) and a linear gradient of acetonitrile was used for elution. The lyophilized sample was injected onto the column and eluted at a flow rate of 1 mL min^{-1} and the eluate was monitored by UV detection at 215, 254 and 280 nm.

MALDI-TOF mass spectrometry: The masses of the purified peptides were determined by MALDI-TOF mass spectrometry with the aid of a Voyager-DE Biospectrometry workstation fitted with a 337 nm nitrogen laser. The purified fraction (0.5 μL) was mixed with same amount of matrix solution (saturated sinapinic acid in 50% acetonitrile) before spotting of the mixture on a MALDI plate. To obtain a good signal to noise ratio, 100 single-shot spectra were collected.

Amino terminal sequencing: Amino terminal sequencing of the purified peptides was performed by automated Edman degradation with a Perkin–Elmer Applied Biosystems 494 pulsed-liquid phase protein sequencer (Procise) with an online 785 A PTH-amino acid analyser.

In vitro crystal growth: Crystals were grown on glass cover slips placed in small Petri dishes. $CaCl_2$ solution (3 mL, 25 mM) and appropriate volumes of $MgCl_2$ solution (2.5 M) were introduced into each Petri dish to provide a final concentration of Mg/Ca 1:1. The crystallization time was varied from 30 minutes to 48 h. The Petri dishes containing the crystal growth solutions were covered with aluminium foil with a few pinholes in the top and placed in a closed desiccator. Crystals were grown by the slow diffusion of gases released by the sublimation of ammonium carbonate placed inside the desiccator.[27] To study the effect of the SOM on the $CaCO_3$ crystallization, aliquots of the lyophilized crude extract (100 μg mL^{-1}) dissolved in $CaCl_2$ solution (25 mM) were added to the crystallization media containing the required amounts of $MgCl_2$ solution (2.5 M). Crystals were also grown in the presence of Bovine Serum Albumin (BSA) as a negative control in the place of the SOM. After crystallization, the slides were carefully lifted from the crystallization vessels, rinsed gently with Millipore (0.22 micron) water, air dried at room temperature and saved for further analyses. The morphology of the crystals was investigated by SEM after mounting of the samples on an aluminium stub and sputter-coating with gold to increase conductivity during the measurement. The samples were further characterized by FTIR spectroscopy after powdering of the samples and their incorporation into KBr pellets.

Acknowledgements

The authors thank the Agency of Science, Technology and Research (ASTAR), Singapore, National University of Singapore (NUS) for funding support for this project. J.C.W. and D.E.M. were supported in part by grants from the US Dept. of Energy (DE-FG03-02ER46006), the Institute for Collaborative Biotechnologies through grant DAAD19-03-D-0004 from the US Army Research Office, NASA (University Research, Engineering and Technology Institute on Bio Inspired Materials (BIMat) under award Nos. NCC-1-02037 and NAG1-01-003), the NOAA National Sea Grant College Program, US Department of Commerce (NA36RG0537, Project R/MP-92) through the California Sea Grant College System, and the MRSEC Program of the National Science Foundation under award No. DMR-96-32716 to the UCSB Materials Research Laboratory.

[1] S. Mann, *Angew. Chem.* **2000**, *112*, 3532–3548; *Angew. Chem. Int. Ed.* **2000**, *39*, 3392–3406.
[2] S. Weiner, L. Addadi, *J. Mater. Chem.* **1997**, *7*, 689–702.
[3] A. M. Belcher, X. C. Wu, R. J. Christensen, P. K. Hansma, G. D. Stucky, D. E. Morse, *Nature* **1996**, *381*, 56–58.
[4] L. Addadi, S. Weiner, *Angew. Chem.* **1992**, *104*, 159–176; *Angew. Chem. Int. Ed. Engl.* **1992**, *31*, 153–169.
[5] a) E. Savassi, *Functional Morphology of the Invertebrate Skeleton*, Wiley, **1999**, p. 567; b) Y. Oaki, H. Imai, *Small* **2006**, *2*, 66–70.
[6] A. B. Smith, *Skeletal Biomineralization: Patterns, Processes and Evolutionary Trends, AGU Short Course in Geology*, **1989**, *Vol. 5*, 117–147.
[7] J. Aizenberg, G. Hendler, *J. Mater. Chem.* **2004**, *14*, 2066–2072.
[8] J. Aizenberg, A. Tkachenko, S. Weiner, L. Addadi, G. Hendler, *Nature* **2001**, *412*, 819–822.
[9] S. Raz, S. Weiner, L. Addadi, *Adv. Mater.* **2000**, *12*, 38–42.
[10] G. Falini, M. Gazzano, A. Ripamonti, *Chem. Commun.* **1996**, 1037–1038.
[11] G. Falini, S. Fermani, M. Gazzano, A. Ripamonti, *J. Mater. Chem.* **1998**, *8*, 1061–1065.
[12] E. Loste, R. M. Wilson, R. Seshadri, F. C. Meldrum, *J. Cryst. Growth* **2003**, *254*, 206–208.
[13] N. Wada, K. Yamashita, T. Umegaki, *J. Colloid Interface Sci.* **1999**, *212*, 357–364.
[14] U. Magdans, H. Gies, *Eur. J. Mineral.* **2004**, *16*, 261–268.
[15] F. H. Wilt, *J. Struct. Biol.* **2004**, *134*, 56–66.
[16] P. L. O'Neill, *Science* **1981**, *213*, 646–648.
[17] Y. Politi, T. Arad, Y. Klein, S. Weiner, L. Addadi, *Science* **2004**, *306*, 1161–1164.
[18] a) J. R. Goldsmith, L. D. Graf, H. C. Heard, *American Mineralogist* **1961**, *46*, 453–457; b) J. R. Goldsmith, L. D. Graf, *American Mineralogist* **1958**, *43*, 84–101; c) M. E. Bottcher, P. L. Gehlken, D. F. Steele, *Solid State Ionics* **1997**, *101–103*, 1379–1385.
[19] Y. Dauphin, *J. Biol. Chem.* **2003**, *278*, 15168–15177.
[20] F. C. Meldrum, *Int. Mater. Rev.* **2003**, *48*, 187–225.
[21] L. Addadi, S. Raz, S. Weiner, *Adv. Mater.* **2003**, *15*, 959–970.
[22] E. Beniash, J. Aizenberg, L. Addadi, S. Weiner, *Proc. R. Soc. London Ser. B* **1997**, *264*, 461–465.
[23] G. Falini, S. Fermani, M. Gazzano, A. Ripamonti, *Chem. Eur. J.* **1997**, *3*, 1807–1814.
[24] S. Raz, P. C. Hamilton, F. H. Wilt, S. Weiner, L. Addadi, *Adv. Funct. Mater.* **2003**, *13*, 480–486.
[25] K. J. Davis, P. M. Dove, J. J. De Yoreo, *Science* **2000**, *290*, 1134–1137.
[26] D. Kralij, J. Kontrec, L. Brecevic, G. Falini, V. N. Laslo, *Chem. Eur. J.* **2004**, *10*, 1647–1656.
[27] J. Aizenberg, G. Lambert, S. Weiner, L. Addadi, *J. Am. Chem. Soc.* **2002**, *124*, 32–39.

Received: June 13, 2006
Revised: September 9, 2006
Published online: January 5, 2007

